Journal of Hazardous Materials 163 (2009) 136–142

Contents lists available at ScienceDirect

Journal of Hazardous Materials

journal homepage: www.elsevier.com/locate/jhazmat

Simulation of radioelement volatility during the vitrification of radioactive wastes by arc plasma

Imed Ghiloufi*

College of Sciences, Department of Physics, Al-Imam Muhammad bin Saud University, P.O. Box 90950, Riyadh 11623, Saudi Arabia

ARTICLE INFO

Article history:
Received 16 March 2008
Received in revised form 18 June 2008
Accepted 18 June 2008
Available online 5 July 2008

Keywords:
Radioactive wastes
Volatility
Arc plasma
Modeling
Thermodynamics

ABSTRACT

A computer model is used to simulate the volatility of some radioelements cesium (^{137}Cs), cobalt (^{60}Co), and ruthenium (^{106}Ru) during the radioactive wastes vitrification by thermal plasma. This model is based on the calculation of system composition using the free enthalpy minimization method, coupled with the equation of mass transfer at the reactional interface. The model enables the determination of the effects of various parameters (e.g., temperature, plasma current, and matrix composition) on the radioelement volatility. The obtained results indicate that any increase in molten bath temperature causes an increase in the cobalt volatility; while ruthenium has a less obvious behavior. It is also found that the oxygen flux in the carrier gas supports the radioelement incorporations in the containment matrix, except in the case of the ruthenium which is more volatile under an oxidizing atmosphere. For electrolyses effects, an increase in the plasma current considerably increases both the vaporization speed and the vaporized quantities of ^{137}Cs and ^{60}Co. The increase of silicon percentage in the containment matrix supports the incorporation of ^{60}Co and ^{137}Cs in the matrix. The simulation results are compared favorably to the experimental measurements obtained by emission spectroscopy.

1. Introduction

Radioactive wastes are classified into various categories according to their type of emitted radiation. Each category requires a specific treatment, such as storing on the surface, coating in various binders, or conditioning in a vitreous matrix by plasma vitrification [1]. Plasma technology is an effective solution to treat the most toxic wastes like organohalogen wastes, contaminated hospital wastes, fly ashes, and radioactive wastes [2].

Plasma torch technology has been developed to produce temperatures as high as 4000 °C. At these temperatures, any substance is vitrified, i.e., reduced in volume and transformed into a glassy obsidian whose leachability is many times less than bottle glass. Thermal plasma technology takes the advantages to incinerate the combustible parts of radioactive wastes for volume reduction and to vitrify the noncombustible counter parts simultaneously into glassy slags with very low leaching rate [3,4].

The vitrified may contain a proportion more or less important in the crystallized phase: the proportion between vitreous phases and crystallized phases depending on the waste composition and the cooling method of the liquid during the treatment [5]. The properties of the glassy slags depend on many parameters like treatment temperature, waste composition, etc. For example the density and the hardness of vitrified decrease when the heat treatment temperature increases, whereas its porosity and its water absorption increase with heat treatment temperature [6].

The problem of radioactive wastes vitrification by arc plasma is the volatility of radioelements (e.g., ^{60}Co, ^{137}Cs, and ^{106}Ru.) which end up leaving the furnace and reaching the filtering units and the washing column [7]. Hence, the volatility of these elements needs to be controlled during the treatment. Experimentally, radioelements volatility during the plasma vitrification of radioactive wastes is measured using emission spectroscopy diagnostic. During such diagnostic, the variations over time of the molar ratio of Cs/Ar, Co/Ar, and Ru/Ar are measured and the effect of oxygen and hydrogen on radioelement volatility is investigated [8].

The main objective of this work is to study the behaviors of radioelements like (^{137}Cs, ^{60}Co, and ^{106}Ru) during the arc-transferred plasma vitrification of radioactive wastes using a computer code. This code combines three important factors: (a) the thermal effects during liquid–gas equilibrium at the interface, (b) the diffusion phenomena in the gas phase, and (c) the electrolyses effects, which occur between the electrodes and the liquid bath. Precisely, the work aims at the determination of the effects induced on the radioelement volatility by the liquid bath temperature, by the plasma current, by the matrix composition, and by the oxygen pressure in the carrier gas.

* Tel.: +966 509407164; fax: +966 12591616.
E-mail address: ghiloufimed@yahoo.fr.

0304-3894/$ – see front matter © 2008 Elsevier B.V. All rights reserved.
doi:10.1016/j.jhazmat.2008.06.110

Table 1
Composition of basalt

	Elements							
	Mg	K	Na	Ca	Si	Al	Fe	Ti
Chemical form	MgO	K_2O	Na_2O	CaO	SiO_2	Al_2O_3	FeO	TiO_2
% in mass	10.2	1.2	3	8.8	50.4	12.2	11.9	2.2
Cation mole number	0.253	0.021	0.154	0.157	0.838	0.239	0.165	0.034

2. Model equations

In the model, the species distribution in the liquid and gas phases is obtained iteratively using the calculation of system composition coupled with the mass transfer equation. The quantity of matter formed in the gas phase is distributed into three parts: the first part is in equilibrium with the bath, the second part is diffused in the diffusion layer, and the third part is retained by the bath under the electrolyses effects. The gas composition at the surface is thus modified. It is not the result of a single equilibrium liquid–gas, but instead, it is the outcome of a dynamic balance comprising: a combined action of reactional balances, electrolyses effects, and diffusive transport.

The system composition at equilibrium is calculated according to the principle of total free enthalpy minimization. The minimization has two constraints: the matter conservation [9] and the proper choice of the partial pressure of oxygen [10]. This model determines, for a given temperature and total pressure, the equilibrium composition of a closed system. The model can handle 20 elements, 99 species, and 10 different phases as a maximum.

The matter conservation equation of oxygen or the mass transfer equation at the interface is given by [11]

$$\sum_{j=1}^{L} \vartheta_j (J^{G}_{M_j}) - \sum_{i=1}^{M_1} a_{ik} J^{G}_{i} - \frac{1}{A} \sum_{j=1}^{L} n_{M_j} \frac{d\vartheta_j}{dt} = 0 \quad (1)$$

where ϑ_j and a_{ik} are, respectively, the stoichiometric coefficient of a metal j and of oxygen in species i. n_{M_j} (mol) represents the total mole number of metal j in the liquid phase, and $J^{G}_{M_j}$ (mol s^{-1} cm^{-2}) is the equivalent density of molar flux of a metal j from the gas phase. The flux density of a gas species i (J^{L}_{i}) lost in each iteration is given by

$$J^{L}_{i} = J^{D}_{i} - J^{R}_{i} \quad (2)$$

where J^{D}_{i} and J^{R}_{i} are, respectively, the diffusion flux density and the retained flux by the bath for the gas species i.

The diffusion flux density for a gas species i is given by [12,13]

$$J^{D}_{i}\ (\text{mol s}^{-1}\,\text{cm}^{-2}) = -\frac{D_i}{RT}\left(\frac{p^{x}_{i} - p^{w}_{i}}{\delta_i}\right) + J_T \frac{p^{w}_{i}}{P} \quad (3)$$

where p^{w}_{i} (Pa) and p^{x}_{i} (Pa) represent the partial pressure of species i, at the interface and in the carrier gas, respectively. J_T (mol s^{-1} cm^{-2}) is the total mass flux density (with $J_T = \sum_{i=1}^{L-1} J^{G}_{i}$), P is the total pressure, δ_i (cm) is the boundary layer thickness; D_i (cm^2 s^{-1}) is the diffusion coefficient. Here, argon is used as a carrier gas which, in the plasma conditions, is supposed to be an inert gas with molar flux density zero (i.e., $J^{G}_{Ar} = 0$).

For temperatures less than 1000 K, the diffusion coefficients for current gases (oxygen, argon, nitrogen, etc.) are known. For temperatures higher than 1000 K, these coefficients can be calculated according to level 1 of the Chapman–Enskog approximation [14]. However, for the other gas species (e.g., the metal vapor and radioelements), the parameters of the intermolecular potential remain unknown regardless of the interaction potential used. This makes the determination of the reduced collision integral impossible. Therefore, the diffusion coefficients are calculated using the method developed in [11].

The flux retained by the bath for a gas species i, is given by [15]

$$J^{R}_{i} = \frac{I}{AFv} n^{0}_{i} \quad (4)$$

where I represents the plasma current, $F = 96{,}485$ C mol^{-1} is Faraday's constant, A (cm^2) is the value of the interface surface, v is the valence number of the substance as an ion (electrons per ion), and n^{0}_{i} is the initial mole number of a substance i.

3. Application to radioelements

To simulate the same emission spectroscopy conditions in which the experimental measurement are obtained, the containment matrix used for this study is formed by basalt, and its composition is given in Table 1.

At high temperatures ($T > 1700$ K), in the presence of oxygen and argon, the following species are preserved in the model:

- In the vapor phase: O_2, O, Mg, MgO, K, KO, Na, Na_2, NaO, Ca, CaO, Si, SiO, SiO_2, Al, AlO, AlO_2, Fe, FeO, Ti, TiO, TiO_2, and Ar.
- In the condensed phase: $CaSiO_3$, Ca_2SiO_4, $CaMgSi_2O_6$, $K_2Si_2O_5$, SiO_2, Fe_2SiO_4, Fe_3O_4, FeO, $FeNaO_2$, Al_2O_3, CaO, Na_2O, Na_2SiO_3, $Na_2Si_2O_5$, K_2O, K_2SiO_3, MgO, $MgAl_2O_4$, $MgSiO_3$, Mg_2SiO_4, $CaTiSiO_5$, $MgTi_2O_5$, Mg_2TiO_4, $Na_2Ti_2O_5$, $Na_2Ti_3O_7$, TiO, TiO_2, Ti_2O_3, Ti_3O_5, and Ti_4O_7.

This study focuses on the three radioelements ^{137}Cs, ^{60}Co, and ^{106}Ru. Ruthenium is a high activity radioelement, and it is an emitter of α, β, and γ radiations, with long a radioactive period. However, cesium and cobalt are two low activity radioelements and they are emitters of β and γ radiations with short-periods on the average (less than or equal to 30 years) [16]. To simplify the system, the radioelements are introduced separately in the containment matrix, in their most probable chemical form. Table 2 recapitulates the chemical forms and the mass percentages of the radioelements used in the system. The mass percentages chosen in this study are the same as that used in experimental measurements made by [8].

The addition of these elements to the containment matrix, in the presence of oxygen, leads to the formation of the following species:

- In the vapor phase: Cs, Cs_2, CsK, CsNa, CsO, Cs_2O, Cs_2O_2, Ru, RuO, RuO_2, RuO_3, RuO_4, Co, Co_2, and CoO.
- In the condensed phase: Cs, Cs_2O, Cs_2O_2, Cs_2SiO_3, $Cs_2Si_2O_5$, $Cs_2Si_4O_9$, Ru, CoAl, CoO, Co_2SiO_4, CoSi, $CoSi_2$, Co_2Si, and Co.

Table 2
Chemical forms and mass percentages of radioelement

	Radioelement		
	^{137}Cs	^{60}Co	^{106}Ru
Most probable chemical form	Cs_2O	CoO	Ru
% in mass	10	10	5

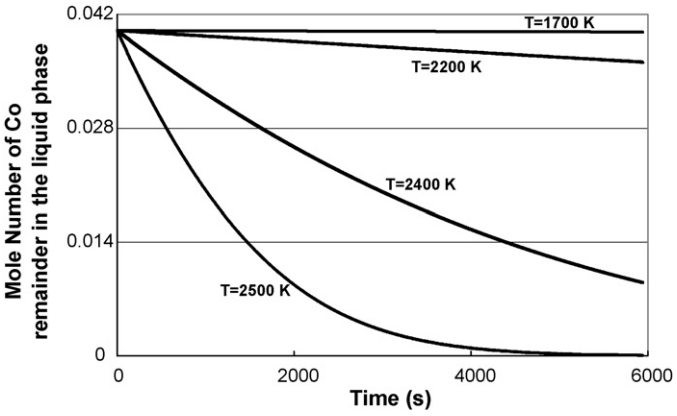

Fig. 1. Influence of temperature on Co volatility.

These species are selected with the assistance of the HSC computer code [17]. In the simulation, the selected formation free enthalpies of species are extracted from the tables of [18–20].

4. Simulation results

4.1. Temperature influence

To have the same emission spectroscopy conditions in which the experimental measurement are obtained [8], in this study the partial pressure of oxygen in the carrier gas P_{O_2} is fixed at 0.01 atm, the total pressure P at 1 atm, and the plasma current I at 250 A. Figs. 1 and 2 depict, respectively, the influence of bath surface temperatures on the cobalt and ruthenium volatility. Up to temperatures of about 2000 K, cobalt is not volatile. Beyond this value, any increase of temperature causes a considerable increase in both the vaporization speed and the vaporized quantity of ^{60}Co. This behavior was also observed for ^{137}Cs [15]. Contrarily to cobalt, ruthenium has a different behavior with temperature. For temperatures less than 1700 K and beyond 2000 K, ruthenium volatility increases with temperature increases. Whereas in the temperature interval between 1700 K and 2000 K, any increase of temperature decreases the ^{106}Ru volatility.

To better understand this Ru behavior, it is necessary to know its composition at different temperatures. Table 3 presents the mole numbers of Ru components in the gas phase at different temperatures obtained from the simulation results. The first observation that can be made is that the mole numbers of Ru, RuO, and RuO_2 increase with temperature, contrary to RuO_3 and RuO_4 whose mole numbers decrease with increasing temperatures. These results are logical because the formation free enthalpies of Ru, RuO, and RuO_2 decrease with temperature. Therefore, these species become more stable when the temperature increases, while is not the case for RuO_3 and RuO_4. A more interesting observation is that at temperatures between 1700 K and 2000 K the mole numbers of Ru, RuO, and RuO_2 increase by an amount smaller that the amount of decrease of the mole numbers of RuO_3 and RuO_4 resulting in an overall reduction of the total mole numbers formed in the gas phase. At temperature between 2000 K and 2500 K the opposite phenomenon occurs.

Table 3
Mole numbers of Ru components in the gas phase at different *temperatures*

	Species				
	Ru	RuO	RuO_2	RuO_3	RuO_4
Mole numbers					
1700 K	6.10^{-14}	3.10^{-10}	4.10^{-6}	7.10^{-5}	1.10^{-6}
2000 K	5.10^{-11}	2.10^{-8}	1.10^{-5}	3.10^{-5}	1.10^{-7}
2500 K	1.10^{-7}	2.10^{-6}	8.10^{-5}	1.10^{-5}	2.10^{-8}

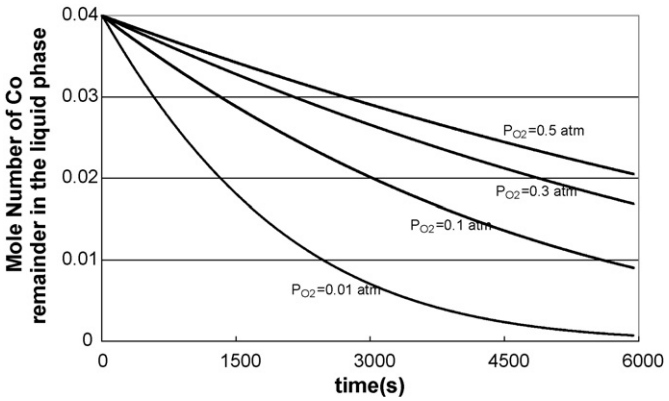

Fig. 3. Influence of the atmosphere nature on the Co volatility.

4.2. Effect of the atmosphere

The furnace atmosphere is supposed to be constantly renewed with a composition similar to that of the carrier gas made up of the mixture argon/oxygen. For this study, the temperature is fixed at 2500 K, the total pressure P at 1 atm and the plasma current I at 250 A. Figs. 3 and 4 present the results obtained for ^{60}Co and ^{106}Ru as a function of P_{O_2}.

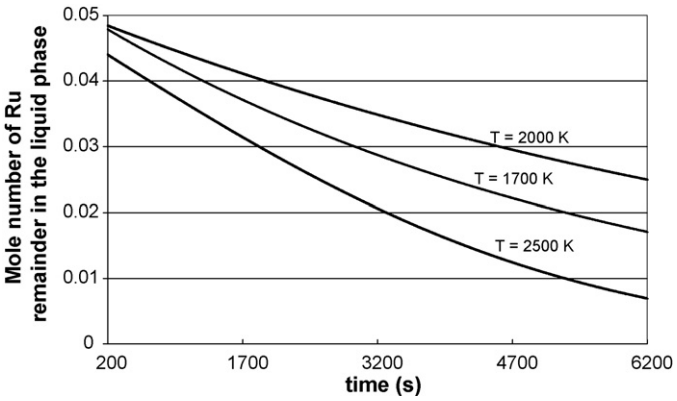

Fig. 2. Influence of temperature on Ru volatility.

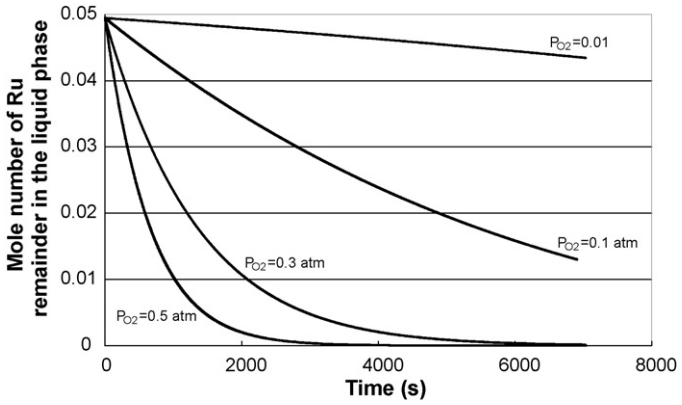

Fig. 4. Influence of the atmosphere nature on the Ru volatility.

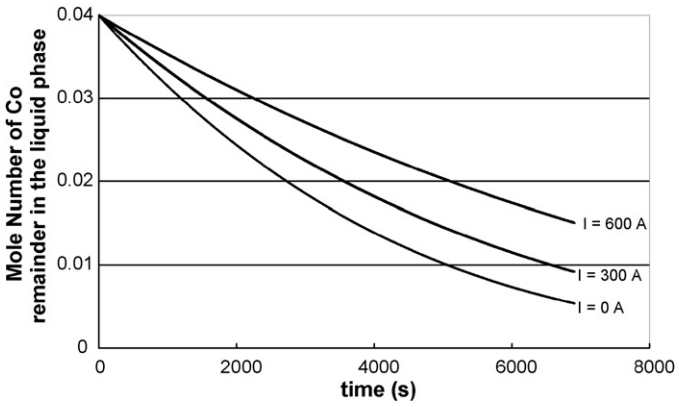

Fig. 5. Influence of current on Co volatility.

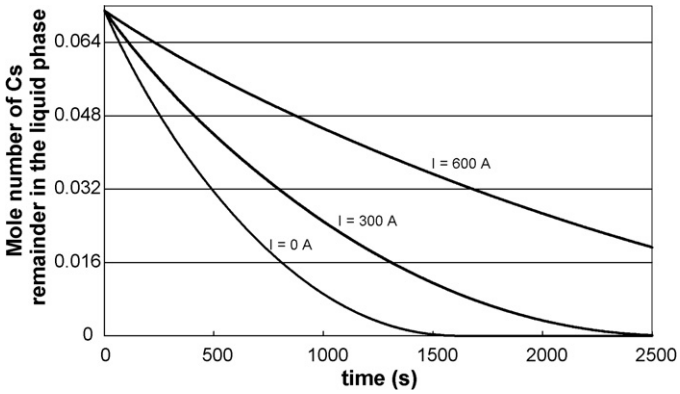

Fig. 6. Influence of current on Cs volatility.

For ^{60}Co, a decrease in the vaporization speed and in the volatilized quantity can be noticed when the quantity of oxygen increases, i.e., when the atmosphere becomes more oxidizing. The presence of oxygen in the carrier gas supports the incorporation of cobalt in the containment matrix. The same behavior is observed in the case of ^{137}Cs in accordance with P_{O_2} [15].

When studying the ruthenium volatility presented in the curves of Fig. 4 it is found that, contrary to ^{60}Co, this volatility increases with the increase of the oxygen quantity. This difference in the ruthenium behavior compared to cobalt can be attributed to the redox character of the majority species in the condensed phase and gas in equilibrium. For ^{60}Co, the oxidation degree of the gas species is smaller than or equal to that of the condensed phase species, hence the presence of oxygen in the carrier gas supports the volatility of ^{60}Co. Whereas ^{106}Ru, in the liquid phase, has only one form (Ru). Hence, the oxidation degree of the gas species is greater than or equal to that of liquid phase species and any addition of oxygen in the gas phase increases its volatility.

4.3. Influence of current

To study the influence of the current on the radioelement volatility, the temperature and the partial pressure of oxygen are fixed, respectively, at 2200 K and at 0.2 atm, whereas the plasma current is varied from 0 A to 600 A. Figs. 5 and 6 depict the influence of plasma current on the cobalt and cesium volatility. The curves of these figures indicate that the increase of the plasma current considerably increases both the vaporization speed and the vaporized quantity of ^{60}Co and ^{137}Cs.

In the model, the electrolyses effects are represented by the ions flux retained by the bath, given by Eq. (4), which depends essentially on the plasma current. As the evaporation kinetics decrease with intensity current, the bath is in cathode polarization which prevents ^{60}Co and ^{137}Cs from leaving the liquid phase. Theses results assert the validity of Eq. (4) used by this computer code and conforms with the experimental results obtained by spectroscopy emission [8]. The same behavior is observed in the case of ^{106}Ru as a function of plasma current.

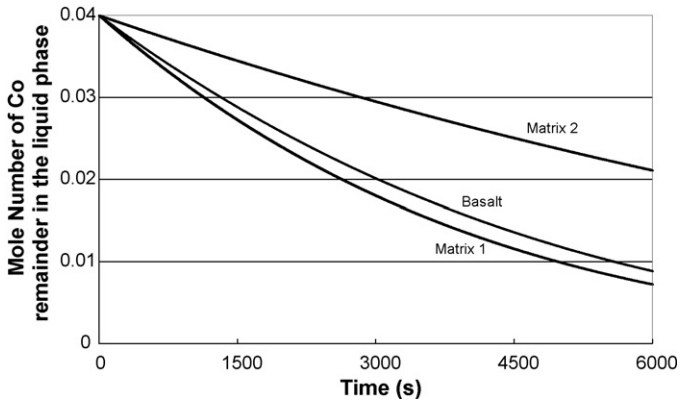

Fig. 7. Influence of matrix composition on Co volatility.

4.4. Influence of matrix composition

Three matrices are used in this study and their compositions are given in Table 4. Matrix 1 is obtained by the elimination of 29 g of silicon for each 100 g of basalt, whereas matrix 2 is obtained by the addition of 65 g of silicon for each 100 g of basalt, and matrix 3 is basalt. Figs. 7 and 8 depict the influence of containment matrix

Table 4
Containment matrices compositions used for Co and Cs

	Elements							
	Mg	K	Na	Ca	Si	Al	Fe	Ti
Matrix 1								
% in mass	14.4	1.7	4.2	12.5	30.1	17.2	16.8	3.1
Mole number	0.356	0.03	0.217	0.221	0.5	0.337	0.232	0.189
Matrix 2								
% in mass	6.18	0.72	1.8	5.3	70	7.39	7.21	1.33
Mole number	0.153	0.01	0.093	0.095	1.918	0.144	0.1	0.08
Basalt								
% in mass	10.2	1.2	3	8.8	50.4	12.2	11.9	2.2
Mole number	0.253	0.021	0.154	0.157	0.838	0.239	0.165	0.034

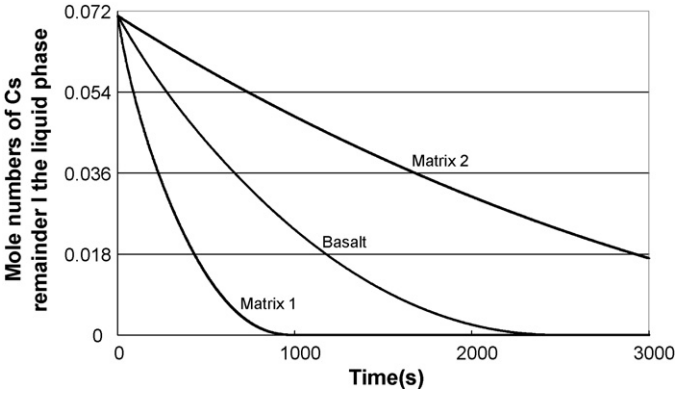

Fig. 8. Influence of matrix composition on Cs volatility.

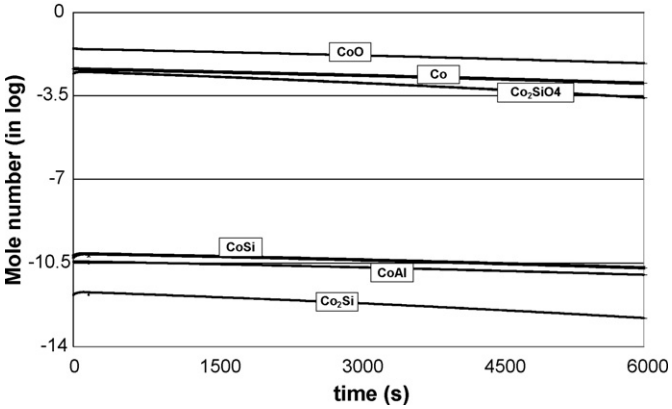

Fig. 10. Variation of the mole numbers of Co composition in the liquid phase.

composition, respectively, on the cobalt and cesium volatility. The increase of silicon percentage in the containment matrix supports the incorporation of ^{60}Co and ^{137}Cs in the matrix.

For ^{137}Cs, the increase of silicon percentage in the containment matrix is accompanied by an increase in mole numbers of $Cs_2Si_2O_5$ and $Cs_2Si_4O_9$ in the condensed phase. The presence of these two species in addition to Cs_2SiO_3 in significant amounts (between 10^{-3} mol and 10^{-2} mol) prevents Cs from leaving the liquid phase and reduces its volatility. For cobalt, the increase of silicon percentage in the system supports the confinement of ^{60}Co in the condensed phase in the Co_2SiO_4 form. Ruthenium is not considered in this study because, in the liquid phase, it has only the Ru form and any modification in the containment matrix has no effect on its volatility.

4.5. Distribution of Co and Ru on its elements during the treatment

Figs. 9 and 10 depict the distribution of cobalt components on the liquid and gas phases. In the gas phase, cobalt exists essentially in the form of Co and, to a smaller degree, in the CoO form. In the liquid phase, cobalt is found in quasi totality in CoO, Co, and Co_2SiO_4 forms.

Fig. 11 presents the distribution of ruthenium components on the liquid and gas phases. In the gas phase, ruthenium exists essentially in the form of RuO_2 and, to a smaller degree, in the form of RuO_3 and RuO, whereas Ru and RuO_4 exist in much smaller quantities compared to the other forms. In the liquid phase, ruthenium has only the Ru form.

5. Comparison with the experimental results

The experimental setup is constituted of a cylindrical furnace, which supports a plasma device with twin-torch transferred arc system. The two plasma torches have opposite polarity. The reactor and the torches are cooled with water under pressure by two completely independent circuits. Argon is introduced at the tungsten cathode and the copper anode while oxygen, helium, and hydrogen are injected through a water-cooled pipe [21].

To perform spectroscopic diagnostic above the molten surface, a water-cooled stainless-steel crucible is placed under the coupling zone of the twin plasma torches. This crucible is filled with basalt and 10% in oxide mass of Cs. On the cooled walls, the material does not melt and, hence, runs as a self-crucible. The intensities of the Ar line (λ = 667.72 nm) and the Cs line (λ = 672.32 nm) are measured by using an optical emission spectroscopy method (Fig. 12). The molar ratio Cs/Ar is deduced from the intensity ratio of the two lines [8].

Fig. 13 shows the code results in comparison with the experimental measurements. This figure reveals that the experimental and simulation results are relatively close. The small difference between the simulation results and the experimental measurements can be attributed to the measurements errors. In fact, the estimated error committed on the measurement of the ratio Cs/Ar is around 10% [8]. The model calculations assumed a bath fully melted and homogeneous from the beginning (t = 0 s), while in practice the inside of the crucible is not fully melted and there is a progress of fusion front that allows a permanent alimentation of

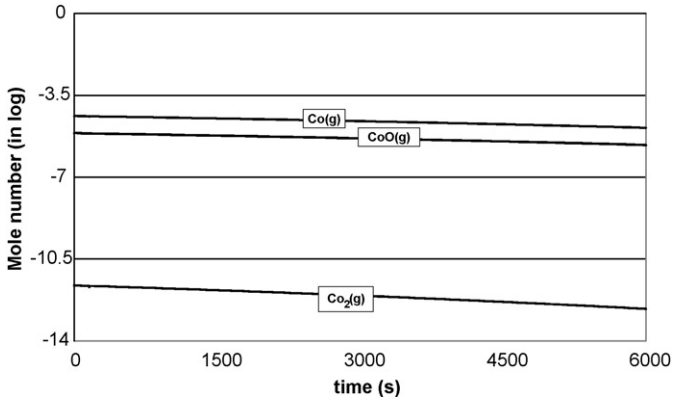

Fig. 9. Variation of the mole numbers of Co composition in the gas phase.

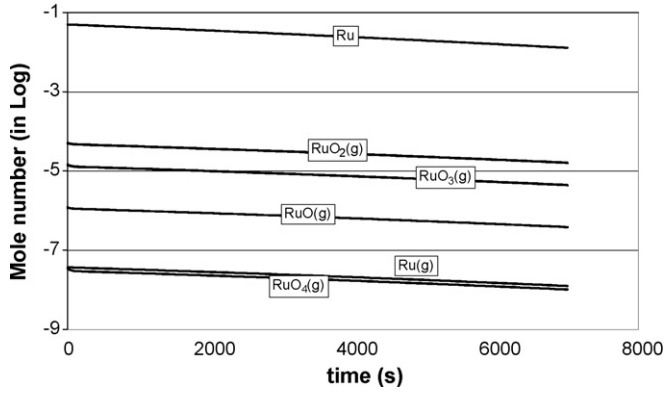

Fig. 11. Variation of the mole numbers of Ru composition in the gas and liquid phases.

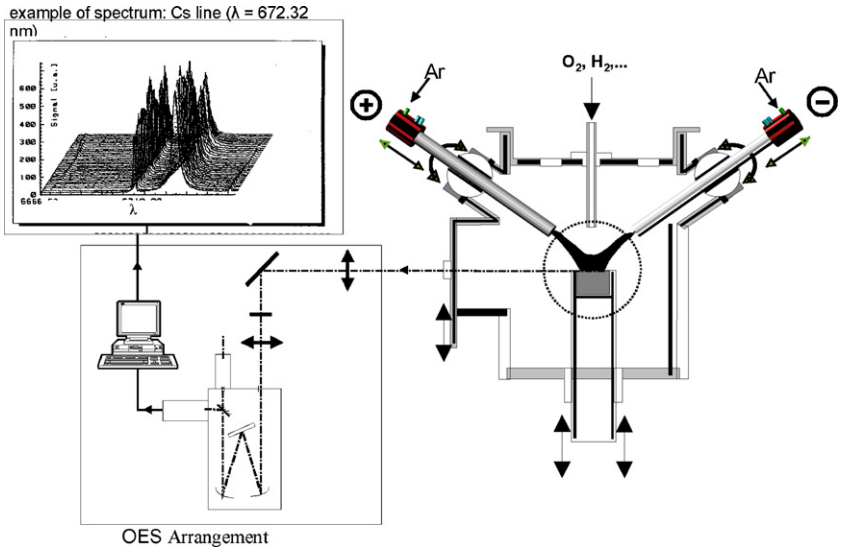

Fig. 12. Experimental set-up.

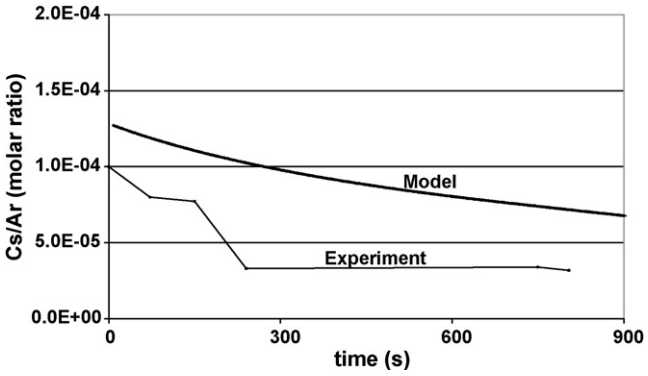

Fig. 13. Comparison between the simulation and experimental results.

the liquid phase in elements from the solid. These causes explain the perturbation of the experimental measurements and the large gap between these measurements and the results obtained by the model in the first few minutes.

6. Conclusions

The objective of this study is to improve the evaporation phenomena related to the radioelements volatility and to examine their behavior when they are subjected to a heat treatment such as vitrification by arc plasma. The main results show that up to temperatures of about 2000 K, cobalt is not volatile. For temperatures higher than 2000 K, any increase in molten bath temperature causes an increase in the cobalt volatility. Ruthenium, however, has a different behavior with temperature compared to cobalt. For temperatures less than 1700 K and beyond 2000 K, ruthenium volatility increases when temperature increases. Whereas in the temperature interval from 1700 K to 2000 K, any increase of temperature decreases the ^{106}Ru volatility. Oxygen flux in the carrier gas supports the radioelement incorporations in the containment matrix, except in the case of the ruthenium which is more volatile under an oxidizing atmosphere. For electrolyses effects, an increase in the plasma current considerably increases both the vaporization speed and the vaporized quantities of ^{137}Cs and ^{60}Co. The increase of silicon percentage in the containment matrix supports the incorporation of ^{137}Cs and ^{60}Co in the matrix. The comparison between the simulation results and the experimental measurements reveals the adequacy of the computer code.

References

[1] A. Jouan, La Vitrification des Déchets, une Contribution au Respect de notre Terre, Verre, vol. 7, 2001.
[2] B. Guihard, Industrial and environmental applications of non transferred plasma, in: International Conference on Incineration and Thermal Treatment Technologies, New Orleans, USA, 2002.
[3] C.C. Tzeng, Y.Y. Kuo, T.F. Huang, D.L. Lin, Y.J. Yu, Treatment of radioactive wastes by plasma incineration and vitrification for final disposal, J. Hazard. Mater. 58 (1998) 207–220.
[4] B.Y. Min, Y. Kang, P.S. Song, W.K. Choi, C.H. Jung, W.Z. Oh, Study on the vitrification of mixed radioactive waste by plasma arc melting, J. Ind. Eng. Chem. 13 (1) (2007) 57–64.
[5] P. Frugier, Altération des vitrifiats de REFIOM: influence des variations de composition et étude du terme source. Ph.D. Thesis, Université de Montpellier, France, 1999.
[6] T.W. Cheng, J.P. Chu, C.C. Tzeng, Y.S. Chen, Treatment and recycling of incinerated ash using thermal plasma technology, J. Waste Manage. 22 (2002) 485–490.
[7] B. Barthelemy, Combustion–vitrification de déchet radioactifs par plasma d'arc: modélisation de la thermique et de la dynamique, Ph.D. Thesis, Université de Limoges, France, 2003.
[8] C. Girold, Incinération/vitrification de déchets radioactifs et combustion de gaz de pyrolyse en plasma d'arc, Ph.D. Thesis, Université de Limoges, France, 1997.
[9] G. Eriksson, E. Rosen, Thermodynamic studies of high temperature equilibria, J. Chem. Scripta 4 (1973) 193–194.
[10] I. Ghiloufi, Modeling of chemical system vaporization at high temperatures: application to the vitrification of fly ashes by plasma, J. High Temp. Mater. Process 12 (1) (2008) 1–10.
[11] I. Ghiloufi, J.M. Baronnet, Simulation of heavy metals volatility during the vitrification of fly ashes by thermal plasma, J. High Temp. Mater. Process 10 (1) (2006) 117–139.
[12] J.M. Badie, X. Chen, G. Flamant, Dynamics of complex chemical system vaporization at high temperature. Application to the vitrification of fly ashes by thermal plasma, J. Chem. Eng. Sci. 52 (23) (1997) 4381–4391.
[13] G. Pichelin, A. Rouanet, Predictive modelling of high-temperature chemical system vaporization under atmospheric pressure, J. Chem. Eng. Sci. 46 (7) (1991) 1635–1649.
[14] J.O. Hirschfelder, C.F. Curtis, R.B. Bird, Molecular Theory of Gases and Liquids, John Willey & Sons, New-York, 1954.
[15] I. Ghiloufi, J. Amouroux, Electrolyses effects on the cesium volatility during thermal plasma vitrification of radioactive wastes, J. High Temp. Mater. Process, (2008), in press.
[16] M. Jorda, E. Revertegat, Les clefs du CEA, n°30, 1995, pp. 48–61.

[17] Outokumpu HSC Chemistry, Chemical Reaction and Equilibrium Modules with Extensive Thermochemical Database, Version 6, 2006.
[18] I. Barin, Thermochemical Data of Pure Substances, VCH, Weinheim/Basel, Switzerland/Cambridge/New York, 1989.
[19] Chase Malcolm, NIST-JANAF, Thermochemical Tables, fourth edition, J. Phys. Chem. Ref. Data, Monograph No. 9, 1998.
[20] Landolt-Bornstein, Thermodynamic Properties of Inorganic Material, Scientific Group Thermodata Europe (SGTE), Springer-Verlag, Berlin-Heidelberg, 1999.
[21] S. Megy, S. Bousrih, J.M. Baronnet, E.A. Ershov-Pavlov, J.K. Williams, D.M. Iddles, Characterization of a twin-torch transferred dc arc, J. Plasma Chem. Plasma Process. 15 (2) (1995) 309–319.